Journal of Materials Chemistry A

Accepted Manuscript

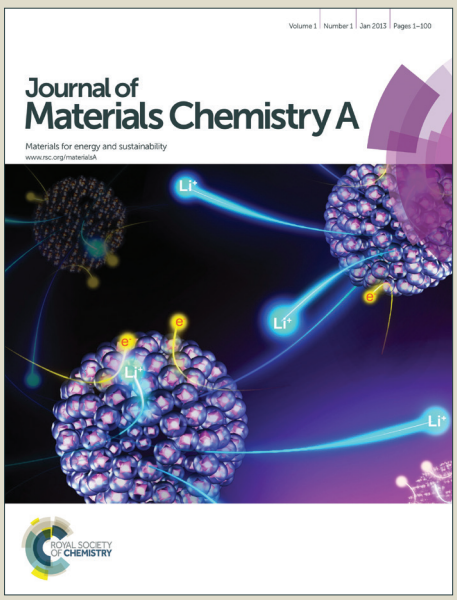

ROYAL SOCIETY OF CHEMISTRY

www.rsc.org/materialsA

Table of contents

Microporous N-doped carbon confined Se as cathode material for advanced Li–Se battery.

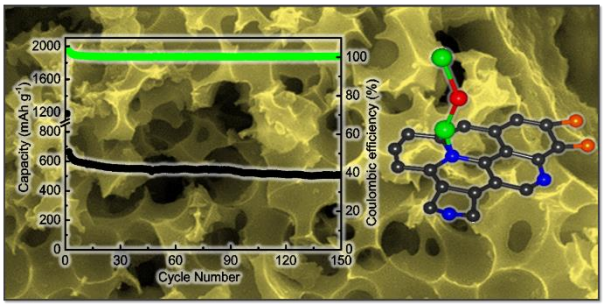

Journal Name

RSCPublishing

ARTICLE

High-Performance Lithium-Selenium Batteries Promoted by Heteroatom-Doped Microporous Carbon

Cite this: DOI: 10.1039/x0xx00000x

Ziqi Yi, Lixia Yuan*, Dan Sun, Zhen Li, Chao Wu, Wenjuan Yang, Yanwei Wen, Bin Shan* and Yunhui Huang*

Received 00th January 2012,
Accepted 00th January 2012

DOI: 10.1039/x0xx00000x

www.rsc.org/

A novel microporous N-doped carbon confined Se composite is developed as cathode material for advanced Li–Se battery. The microporous N-doped carbon is synthesized by carbonization of a ratio-fixed mixture of polypyrrole and KOH. The Se composite cathode delivers a discharge capacity as high as 303 mAh g^{-1} at 20 C and a reversible capacity of 506 mAh g^{-1} at 1 C even after 150 cycles. The superior electrochemical performance can be ascribed to the high electrical conductivity promoted by N-doping and the unique microporous structure of carbonized polypyrrole which creates additional active sites for Li-ion storage. More importantly, we use first-principle calculation to evaluate the influence of heteroatom doping on electrochemical performance, further confirming that the existence of heteroatoms in carbon framework greatly facilitates the interaction between carbon and Li_2Se, which can well explain the excellent cycling performance and rate capability.

Introduction

Lithium-ion batteries (LIBs) are important options for response to the environmental needs for storage of electrical energy that can be coupled to renewable sources such as solar and wind. They can also be used as storage for braking energy for vehicular transport systems. However, given that traditional insertion cathode materials used in LIBs afford a limited gravimetric energy density that cannot meet the requirement of high energy/power density for electric vehicles,[1-3] new generations of cathode material with high capacity and energy density are urgently needed. Sulfur is a promising candidate due to its high theoretical specific capacity (1675 mA h g^{-1}) and theoretical specific energy (2600 Wh kg^{-1}), which is usually combined with a Li anode by forming Li_2S discharge product.[3-8] However, Li-S batteries are plagued by some drawbacks that hinder the practical application. The drawbacks mainly include short cycling lifespan due to dissolution of the intermediate long-chain polysulfides in the electrolyte, and "shuttle effect" occuring during continuous discharge/charge process which leads to low coulombic efficiency.[5] Besides, the sulfur presents low active-material utilization and poor rate capability as a result of its insulting nature. In recent years, many approaches have been devoted to addressing these problems, such as fabricating C-S composites via incorporating sulfur into various porous carbon materials to improve the conductivity and absorb the intermediate polysulfides,[5, 9, 10] modifying the particle surface[11-14] or cell construction,[15, 16] or adjusting the electrolyte composition to suppress the solubility of the intermediate polysulfides.[17] Although remarkable improvements have been achieved, the realization of Li–S batteries is still hindered by the intrinsic drawbacks of sulfur.

Selenium, as a congener of sulfur, has similar chemical properties with sulfur. Selenium can react with lithium to generate selenide, which can be described as $Se + 2Li^+ + 2e^- \rightarrow Li_2Se$. In spite of lower specific capacity (about 675 mAh g^{-1}) than that of S (1675 mAh g^{-1}), the volumetric capacity of Se (3253 mAh cm^{-3} based on 4.82 g cm^{-3}) is comparable to S (3467 mAh cm^{-3} based on 2.07 g cm^{-3}) benefiting from its higher density.[18] Moreover, Se possesses electronic conductivity of 1×10^{-3} S m^{-1}, approximately 20 orders of magnitude higher than S (5×10^{-28} S m^{-1}).[19] Hence it is expected that Se can bring about better rate capability compared with S. The advantages of Se make it become a prospective candidate for high-performance rechargeable batteries. Pioneering work was conducted by Abouimrane et al.;[19] they presented a new class of Se cathode with certain cycling stability; Guo et al. confined selenium in porous carbon,[18] achieving a much longer cycle life and better rate performance. The Se/C cathode can maintain high reversible discharge capacities 4600 mAh g^{-1} with the Coulombic efficiency of nearly 100%. Liu fabricated nanoporous selenium by using nano-$CaCO_3$ as template,[20] which owns a higher capacity and better cycling behavior than bulk Se without any treatment.

Analogous to the sulfur system, Li-Se batteries also suffer from the fast capacity fading, poor cyclability and low coulombic efficiency, and carbon matrix also plays an important role in the Se/C composites due to its high conductivity, stability and robust porous structure which can suppress the diffusion of dissolved polyselenides. At present, the published research works mainly focused on adjusting the morphologies and pore structures of the carbon matrices, whereas very few reports concerned the intrinsic textures of the carbon material. The optimization of the carbon material itself can affect the physical and chemical properties of carbon, which can also naturally influence the electrochemical performances of the Se/C composites inevitably. Recently, Qu and his group confined selenium in N-containing hierarchical porous carbon and achieved an improvement in rate capability.[21] Zhang et al. used nitrogen-doped porous carbon nanofiber webs as improved carbon matrix for encapsulating selenium.[22] The corresponding Se/C composite showed good electrochemical performance. The obtained improvements are ususally attributed to the interconnected porous nanostructure, abundant channel structure and high specific surface area, but the heteroatom-doping effect has been largely ignored.

In this work, selenium was confined in N-doped microporous carbon fabricated from carbonized polypyrrole (CP) with KOH as pore-forming agent. The obtained CP possesses hierarchical porous structure with regular macropores and interconnected micropores. Nitrogen and oxygen heteroatoms in CP can enhance the chemical adsorption of Li_2Se in the microporous carbon framework, which was verified by first-principle calculation. The Se-CP cathode shows remarkable cycling performance in carbonate-based electrolyte. At 1 C, the reversible capacity maintains 462 mAh g^{-1} after 150 cycles with a capacity retention of 70%. Such Se-CP cathode also exhibits an excellent rate capability. When the current density increases to 20 C, it delivers a capacity higher than 300 mAh g^{-1}, about half of the theoretical value, affording huge advantages in fast discharge/charge application. The electrochemical performances of the Se-CP cathode in the ether-based electrolyte are also demonstrated.

Experimental

Synthesis of PPy

In a typical procedure, 7.3 g cetrimonium bromide (CTAB, $(C_{16}H_{33})N(CH_3)_3Br$) was dissolved in 120 mL HCl solution (1 mol L^{-1}), and then cooled down to 0–5 °C. Then, 13.7 g ammonium persulfate was added; the solution became milky immediately. After being magnetically stirred for 30 min, 8.3 mL pyrrole monomer was added into the as-formed reactive template solution. A black deposit was obtained after being stirred for another 24 h. The precipitate was washed with 1 mol L^{-1} HCl solution and deionized water for several times till the filtrate became colorless and neutral, followed by dehydration in an oven at 80 °C.

Synthesis of carbonized PPy (CP)

CP was synthesized by carbonization of polypyrrole with KOH. Briefly, polypyrrole and KOH was well mixed at weight ratio of 1:3. The mixture was heated up to 600 °C at a heating rate of 3 °C min^{-1} for 1 h under N_2 atmosphere. Then the solid product was washed with 1 mol L^{-1} HCl solution and deionized water till the filtrated solution became neutral. Then the sample was dried overnight at 80 °C in an oven.

Synthesis of the composite

To prepare Se–CP composite, 0.6 g CP and 1.8 g Se were ground together. After being heated at 300 °C for 12 h in a stainless steel autoclave, the obtained composite was transferred to a tube furnace and heated at 350 °C for 2 h to remove residual Se on the surface of CP.

Material Characterization

The XRD patterns were measured on an X-ray powder diffractometer (PANalytical X'pert PRO-DY2198, Holland) operating at 40 kV and 40 mA using Cu Kα radiation (λ = 0.15406 nm). The morphology of the samples was observed by scanning electron microscope (SEM, SIRION200) and transmission electron microscopy (TEM, JEOL 2100F). Thermogravimetric analysis (TGA, PerkinElmer) was carried out in argon atmosphere at a heating rate of 10 °C min^{-1} from 25 to 1000 °C. The BET surface area, pore size and volume were analyzed using N_2 absorption on Micrometritics ASAP 2020 analyzer (US). X-ray photoelectron spectroscopy (XPS) was measured by a KRATOS analytical spectrometer (AXIS-ULTRA DLD-600W) using Al Kα (1486.6 eV) X-ray source. Raman spectra measurement was performed on a Horiba JobinYvon LabRAM HR800.

Electrochemical Measurements

The Se–CP electrode was prepared from a mixture of 70 wt% Se–CP composite, 20 wt% super P, 5 wt% carboxy methyl cellulose (CMC) and 5 wt% styrene butadiene rubber (SBR) in deionized water. The homogeneous slurry was coated onto an aluminum foil and dried in a vacuum oven at 60 °C for 24 h. 1 mol L^{-1} $LiPF_6$ dissolved in a mixture solvent of ethylene carbonate (EC), dimethyl carbonate (DMC) and ethyl methyl carbonate (EMC) (v/v/v=1:1:1) or 1 mol L^{-1} LiTFSI dissolved in a mixture solvent of 1,2-dimethoxyethane (DME) and 1,3-dioxolane (DOL) (v/v=1:1) containing 0.1 mol L^{-1} $LiNO_3$ was used as electrolyte. Li-Se coin cells were assembled in an argon-filled glovebox with oxygen and water contents less than 1 ppm. The as-synthesized Se–CP composite was used as cathode, metallic lithium foil as anode and nickel foam as current collector. Capacity and cycle performance were tested at room temperature on a LAND-CT2001A instrument within a voltage range from 1.0 to 3.0 V. Cyclic voltammetry (CV) was measured by an electrochemistry workstation (PARSTAT 2273) between 1.0 − 3.0 V vs. Li^+/Li at a scanning rate of 0.1 mV s^{-1}.

Results and Discussion

Scheme 1 briefly illustrates the synthesis process for CP and Se-CP composites. Figure 1a shows scanning electron microscopy (SEM) image of CP. It exhibits three-dimensional

(3D) architectural structure with macropores on the surface, which can facilitate the mass transport and provide feasible channel access for molten selenium into the micropores of CP. The micropores can be clearly identified by transmission electron microscopy (TEM) (Fig. 1b). After selenium loading, the Se-CP composite still keeps 3D porous structure similar to pure CP and no selenium accumulation can be observed on the surface (Fig. 1c), indicating that selenium is uniformly dispersed and infused into the micropores inside. The energy dispersive X-ray spectroscopy (EDX) (Fig. 1d) illustrates a high selenium loading in Se-CP. Combined with the TGA result (Fig. S1), the Se content is determined as 60 wt% in the composite. The peaks of Ca and Si are due to the glass substrate used for SEM. The Se and C elemental mappings in Fig. 1e manifest that considerable selenium are well-distributed in the Se-CP framework.

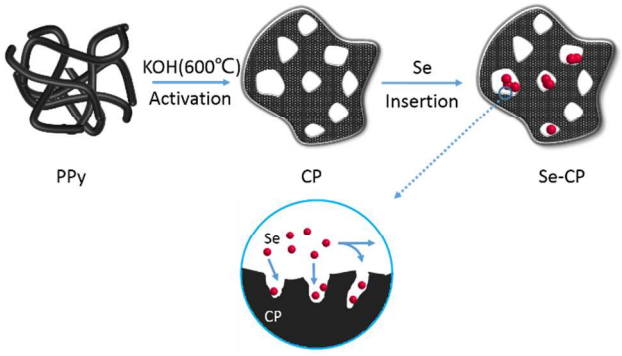

Scheme 1 Schemetic illustration of synthesizing procedure of CP and Se-CP composites.

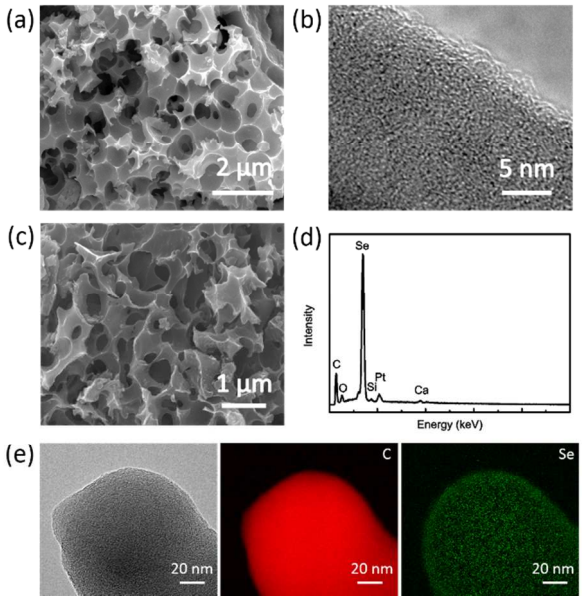

Figure 1 (a) SEM and (b) TEM images of microporous CP, (c) SEM image and (d) EDX pattern of the Se-CP composite, (e) TEM image of Se-CP composite and EDX elemental mapping images of carbon and Se in Se-CP composite.

In order to further confirm the heteroatoms doping and investigate the chemical bonding state of functional CP, X-ray photoelectronic spectron (XPS) measurement was carried out. The overall XPS spectrum on CP in Fig. 2a shows three distinct peaks which represent C 1s, N 1s and O 1s, indicating that the synthesized CP consists of C, N and O. The C 1s (284.7 eV) and N 1s (405.6 eV) peaks are attributed to the carbonization of polypyrrole.[23] The presence of O 1s (531.6 eV) might be assigned to the residual reactant from KOH or physicochemical adsorption of oxygen during synthesis. The spectrum of C 1s in CP displayed in Fig. 2b is divided into four individual peaks corresponding to C-C (284.6 eV), C-N (285.4 eV), C-O (286.5 eV), C=O (288.7 eV).[24] It is thus confirmed that N and O atoms are doped into CP successfully. Three characteristic peaks located at 402.1, 400.4 and 398.9 eV (Fig. 2c) match well with the N 1s spectrum, which can be attributed to pyrrolic (N-5), pyridinic and quaternary N, respectively.[25] This gives an evidence that the N atoms within the five-membered ring of PPy have transformed to N-6 or N-Q partially during the carbonization process. Fig. 2d depicts the XPS survey of high-resolution O 1s spectrum, indicating that there are several O-based groups owing to the incorporation of oxygen during the polymerization process of PPy, including C-O-C ether and C-OH phenol groups.[26] Reactivity and electric conductivity can be enhanced by the presence of heteroatoms in CP.[27] The N content in CP can be estimated as 13.28 wt% by the XPS measurement. The XPS results also affirm that N and O atoms are well introduced into carbon framework and chemically combine with C, which initiates asymmetrical charge and spin density of carbon layer. The resulting charge delocalization in CP provides high conductivity and electrochemical performance.

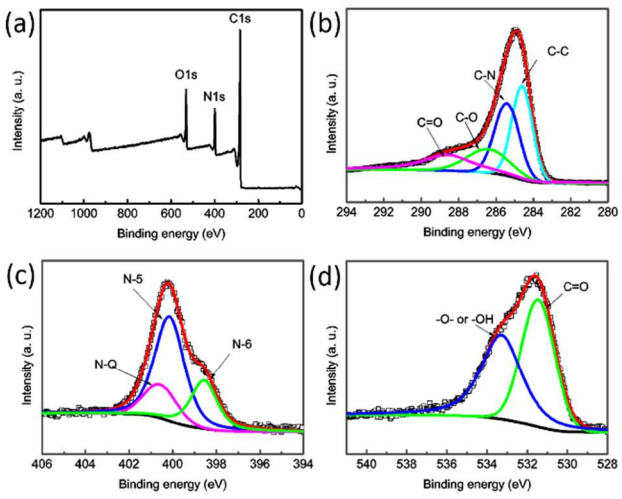

Figure 2 XPS spectra for CP: (a) survey spectrum, and high-resolution spectra of (b) C 1s, (c) N 1s and (d) O 1s.

Figure 3a exhibits the N_2 adsorption-desorption isothermal of the CP. The typical type I isotherm in low-pressure region and a high fraction of micropores in the pore size distribution curve correspond to the microporous structure of CP.

According to the Brunauer-Emmett-Teller (BET) model, the specific surface area is estimated as 3366 m^2 g^{-1}. This tremendous surface area can provide sufficient electrode-electrolyte interface for migration of ions, and hence high rate performance can be attained. Calculated by H-K method （Fig 3b）, the obtained CP has an average pore diameter around 0.5 nm, which agrees well with the TEM image (Fig. 1b). The microporosity of CP is also evidenced by a large pore volume (BJH model) up to 1.75 cm^3 g^{-1}, demonstrating an extraordinary selenium encapsulation. The amount of rearranging Se filler is restricted by microporous space. In our case, one gram CP can accommodate 8.4 g Se. The Se content can be maximized up to 90 wt % if the micropores are fully filled with Se. Since extra space is needed to accommodate volume expansion caused by density difference between Se and discharge product Li_2Se, the Se content in Se-CP is selected at 60 wt%, as further determined by thermogravimetric analysis (TGA) shown in Fig. S1.

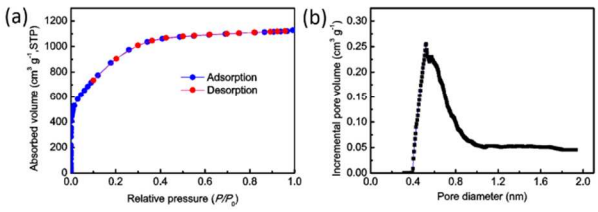

Figure 3 (a) Nitrogen adsorption-desorption isotherms and (b) pore size distribution of CP.

The XRD patterns of CP and Se-CP are shown in Fig. 4. In Fig. 4a, a broad (002) peak appears in both CP and Se-CP, indicative of amorphous state for carbon. No peaks of Se are observed in Se-CP composite, demonstrating that Se exists in a highly dispersed amorphous state. To better understand interaction between Se and CP, the Raman spectra of bulk Se, CP and Se-CP are compared in Fig. 4b. For pure Se, three peaks are observed, among which the peaks at 142.5 and 458.6 cm^{-1} stand for annular Se while the 236.6 cm^{-1} peak represents chain-structured Se.[28] It can be inferred that pure Se is a mixture of annular Se and chain-structured Se.[29] As for CP, the peak at 1333 cm^{-1} (D-band) is attributed to some imperfections like defects, disorders or impurities, while the G-band at 1595 cm^{-1} arises from lattice vibration of graphitic carbon. The graphitization degree of carbon material is usually evaluated according to the intensity ratio of ID to IG. As evaluated from the Raman spectra, the ID/IG ratio for the as-obtained CP is about 0.95, further verifying its partially graphitization degree. The graphitization may ensure good electronic conductivity and facilitate electron transport, and thus result in good electrochemical performance. After encapsulation of Se into microporous structured CP, the intensity of typical Se peaks dramatically decreases, indicating that amorphous Se is embedded successfully into the pores of CP, which agrees well with the XRD patterns.[18, 29] According to the equation of graphitization degree,[30] no peak shift is observed in Se-CP, but a slightly increase occurs in the ID/IG ratio, which may be ascribed to the interaction between the incorporated Se with some unsaturated chemical bonds in CP.

The electrochemical properties were evaluated by coin cells with lithium anode and the as-synthesized Se-CP cathode in both ether- and carbonate-based electrolytes. CV testing was conducted to investigate the kinetic process during discharge and charge. Fig. 5a shows the CV curves of the 1st, 2nd and 5th cycles in ether-based electrolyte at a scan rate of 0.1 mV s^{-1} from 1.0 to 3.0 V. The first cycle shows several ambiguous peaks and one sharp anodic peak at 2.32 V, which related with not only the reduction and oxidation of Se, but also the activation process of cathode and some side reactions between the electrolyte and cathode as well.[31] In the subsequent cycles, three cathodic peaks at 2.17, 2.08 and 1.82 V indicate the conversion of elemental Se to Li_2Se via multiple-phase change. Similar to sulfur system, during lithiation, Se is reduced to soluble long-chain polyselenides Se_n^{2-} ($n \geq 4$), then further reduced to Li_2Se in the following process. In the delithiation process, the three anodic peaks located at 2.04, 2.13 and 2.32 V correspond to the oxidation of Li_2Se to Se with formation of intermediate Se_n^{2-} ($n \geq 4$). Obviously, the Se cathode also suffers from the dissolution issue of polyselenides in ether electrolyte during charge and discharge process. Unlike the case in ether-based electrolyte, the CV curves of Se-CP cathode in carbonate-based electrolyte (Fig. 5b) reveals a strong reduction peak at 1.65 V and oxidation peak at 2.2 V in the first cycle. Interestingly, the cathodic peak shifts to a higher potential in the following cycling and is stabilized at 1.9 V with the anodic peak remaining at 2.2 V. This phenomenon is ascribed to the deformation of Se-CP cathode caused by lithiation in the first cycle. In addition, for the redox process of Se-CP in the carbonate-based electrolyte, only one reduction peak and one oxidation peak can be observed. It seems that there is no soluble Li_2Se_n ($n \geq 4$) formed during the reaction, but only a direct phase change occurs between Se and Li_2Se, which agrees well with Yang's results.[18] Unlike the composites of sulfur confined in the microporous carbon which always show a much lower discharge plateau in the carbonate-based electrolyte than that in the ether-based electrolyte,[10, 32] the Se-CP cathode in the carbon-based electrolyte shows similar reduction potential (1.9 V) to that in the ether-based electrolyte. Furthermore, after the initial activation process, the redox curves of Se-CP cathode in the carbonate-based electrolyte becomes very stable, indicative of a good reversibility, which should be attributed to the excellent ability of CP to confine and stablize both Se and Li_2Se during the electrochemical process.

Table 1 Binding energy of different atoms in CP with Li^+ and Se calculated by first-principle

Structure	N-5 with Se	N-6 with Se	N-Q with Se	O-1 with Se	O-2 with Se	C with Se
Energy/eV	-5.47	-2.54	-3.29	-4.36	-2.53	-2.25
Structure	N-5 with Li^+	N-6 with Li^+	N-Q with Li^+	O-1 with Li^+	O-2 with Li^+	C with Li^+
Energy/eV	-3.92	-4.32	-4.17	-4.2	-4.32	-3.51

More calculation details are provided in supporting information.

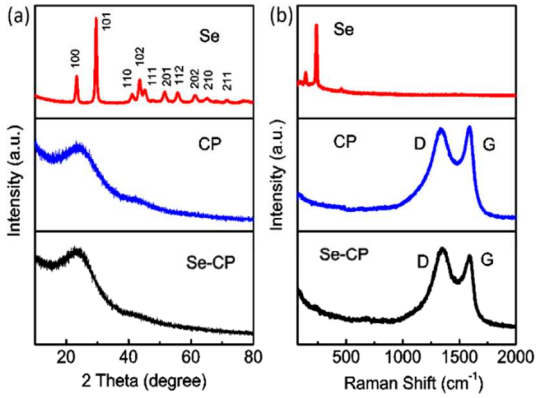

Figure 4 (a) XRD patterns and (b) Raman spectra of Se, CP, and Se-CP.

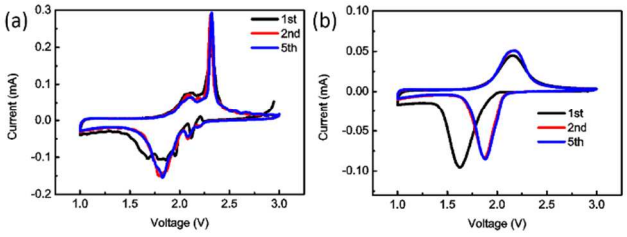

Figure 5 Cyclic voltammograms of Se-CP composite in (a) ether and (b) carbonate-based electrolyte during the 1st, 2nd and 5th cycles.

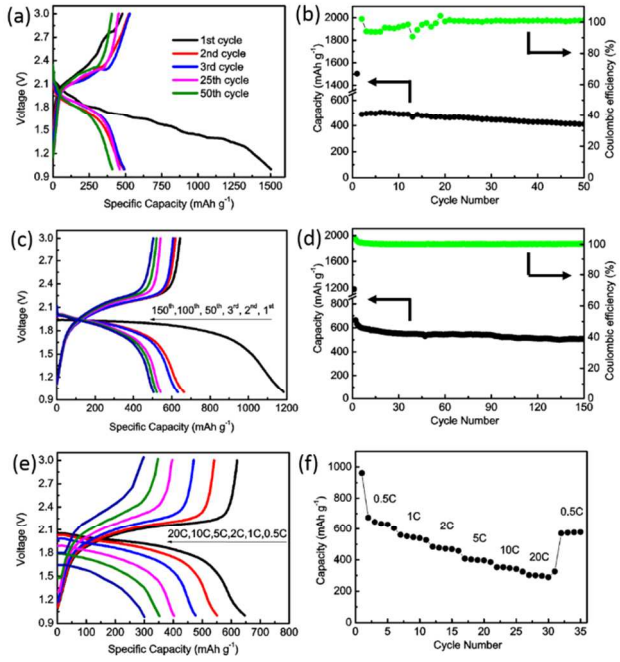

Figure 6 Electrochemical performances of Se-CP composite: (a) charge/discharge profiles in the 1st, 2nd, 3rd, 25th, 50th cycle; and (b) cycling performance and coulombic efficiency in ether-based electrolyte at 1C (c) charge/discharge profiles in the 1st, 2nd, 3rd, 50th, 100th, 150th cycle; and (d) cycling performance and coulombic efficiency in carbonate-based electrolyte at 1C, (e) charge/discharge profiles at different current, and (f) rate capability at various rates from 0.5 to 20 C in carbonate-based electrolyte.

The discharge-charge performance of the Se-CP composite was investigated in both ether- and carbonate-based electrolyte (Fig. 6). Fig. 6a shows discharge/charge profiles of the typical cycles. The Se-CP composite exhibits a very high capacity of 1504 mAh g^{-1} in the first discharging process and a reversible capacity of 480 mAh g^{-1}. High irreversible capacity in the first cycle is commonly observed in Li-S and Li-Se cells when porous carbon is used as supporter,[18] which mainly comes from irreversible reactions between the porous carbon and the

electrolyte. For the ether electrolyte system, there is a little fluctuation with the coulombic efficiency in the initial 20 cycles (Fig. 6b), but it keeps stable in the following cycles. A reversible capacity of 413 mAh g^{-1} is attained after 50 cycles. Higher reversible capacity and better cycle performance are achieved in the carbonate-based electrolyte. In the carbonate-based electrolyte, the Se-CP cathode shows a much higher initial reversible capacity of 664 mAh g^{-1} (Fig. 6c); Even after 150 cycles, a reversible capacity of 506 mAh g^{-1} still remains together with a coulombic efficiency of nearly 100% (Fig. 6d). For the Se-CP cathode in carbonate-based electrolyte, a remarkable rate capability is also attained (Fig. 6e, f); When the current density increases rapidly from 0.5 C to 20 C, the discharge capacity drops slowly. At 20 C, the discharge capacity of Se-CP still reaches up to 303 mAh g^{-1}. If the current density turned back to 0.5 C after cycling at various rates, a reversible capacity of 577 mAh g^{-1} can be recovered. The excellent capacity retention and rate capability should be attributed to the excellent electronic conductivity of Se-CP, which facilitates electron transport and hence results in low polarization.

The excellent electrochemical performance for Se-CP can also relate with heteroatoms doping. Nitrogen shows an electronegativity of 3.5, which is much higher than that of carbon (3.0), meanwhile the nitrogen atom is smaller than carbon atom, therefore N-doping can facilitate lithium insertion[33] and strengthen the interaction between the carbon host and lithium selenide. To elucidate more about the importance of N-doping, we modeled and calculated the binding energy of carbon framework with and without heteroatoms by first-principle calculation. Although this simulation cannot give a precise quantification of the binding strength, it can provide a qualitative understanding of the influence of chemical bond on cycling stability and rate capability for Se-CP. Fig. 7 depicts a brief carbon layer with partially N-doping, in which O-1 and O-2 come from hydroxyl and carbonyl groups, respectively. We computed the binding energy of CP with particles involved in the electrode reactions via first-principle calculation according to the equation described as:

$$E = E_{totle} - E_{CP} - E_X \ (X = Se, Li^+, Li_2Se)$$

Details of calculation are provided in supporting information. The calculated results are summarized in Table 1. We can see that heteroatoms have a stronger interaction with Se atoms and lithium ions to form a chelated coordination structure. This strong binding affinity contributed by the doped heteroatoms can effectively enhance reaction kinetics and facilitate the electrode reaction. Fig. 7 illustrates the interaction between carbon framework and Li_2Se. We select a position where Li_2Se can bond with CP to determine the interaction. The binding energy is found to increase from 1.51 to 1.96 eV after specific carbon positions are replaced by heteroatoms (N-doped), from which we can conclude that the special N-doping structure can suppress the Li_2Se extraction and hence give rise to excellent cycling stability.

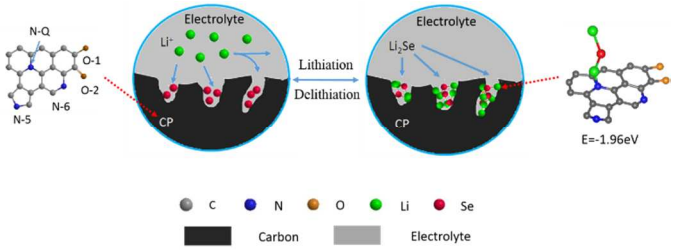

Figure 7 Schematic illustration of charge and discharge mechanism and carbon framework model for first-principle calculation.

Conclusions

A novel Se composite confined in N-doping microporous carbon has been successfully designed and fabricated via a facile melting-diffusion route. As a cathode material for Li-Se battery, the Se-CP composite possesses high stability in low-cost commercial carbonate-based electrolyte and exhibits remarkable cycle stability and rate capability. A high reversible capacity of 462 mAh g^{-1} can be attained at 1 C even after 150 cycles. Combined with first-principle modeling calculation, we ascribe the outstanding performances to the following reasons: (1) the partially graphitized carbon with micropores and large surface area and high conductivity can facilitate the electron transfer and Li-ion diffusion; (2) the robust microstructure can effectively confine Se species during discharging and charging process, promising high stability for the electrode structure; (3) more importantly, doping of heteroatoms N and O in carbon greatly enhances the binding energy between the carbon and Se or Li_2Se, resulting in high electrochemical performance.

Acknowledgements

This work was supported by the Natural Science Foundation of China (Grant Nos. 21273087 and 51361130151) and the 973 program (Grant Nos. 2015CB258400). In addition, the authors thanks the Analytical and Testing Center in Huazhong University of Science and Technology for XRD, SEM, TEM, XPS measurement, and the State Key Laboratory of Material Processing and Die and Mould Technology for TGA measurements.

Notes

State Key Laboratory of Material Processing and Die and Mould Technology, School of Materials Science and Engineering, Huazhong University of Science and Technology, Wuhan, Hubei 430074, China. Tel./fax: +86 2787558421 (Yunhui Huang). Email: huangyh@hust.edu.cn (Yunhui Huang), yuanlixia@hust.edu.cn (Lixia Yuan), bshan@hust.edu.cn (Bin Shan)

† Electronic Supplementary Information (ESI) available: details of first principle calculation; TGA curve of the Se-CP composite. See DOI: 10.1039/b000000x/

References

1. P. G. Bruce, S. A. Freunberger, L. J. Hardwick and J. M. Tarascon, *Nat. Mater.*, 2012, **11**, 19.
2. B. L. Ellis, K. T. Lee and L. F. Nazar, *Chem. Mater.*, 2010, **22**, 691.
3. X. Ji and L. F. Nazar, *J. Mater. Chem.*, 2010, **20**, 9821.
4. J. Shim, K. A. Striebel and E. J. Cairns, *J. Electrochem. Soc.*, 2002, **149**, A1321.

5. X. Ji, K. T. Lee and L. F. Nazar, *Nat. Mater.*, 2009, **8**, 500.
6. B. Jin, J.-U. Kim and H.-B. Gu, *J. Power Sources*, 2003, **117**, 148.
7. S. Wei, H. Zhang, Y. Huang, W. Wang, Y. Xia and Z. Yu, *Energ. Environ. Sci.*, 2011, **4**, 736.
8. Y. Yang, M. T. McDowell, A. Jackson, J. J. Cha, S. S. Hong and Y. Cui, *Nano Lett.*, 2010, **10**, 1486.
9. S. H. Chung and A. Manthiram, *Adv. Mater.*, 2014, **26**, 1360.
10. S. Xin, L. Gu, N. H. Zhao, Y. X. Yin, L. J. Zhou, Y. G. Guo and L. J. Wan, *J. Am. Chem. Soc.*, 2012, **134**, 18510.
11. W. Li, G. Zheng, Y. Yang, Z. W. Seh, N. Liu and Y. Cui, *Proc. Natl. Acad. Sci. U. S. A.*, 2013, **110**, 7148.
12. Y. Fu, Y.-S. Su and A. Manthiram, *Adv. Energ. Mater.*, 2014, **4**, 1300655.
13. Z. Wei Seh, W. Li, J. J. Cha, G. Zheng, Y. Yang, M. T. McDowell, P. C. Hsu and Y. Cui, *Nat. Commun.*, 2013, **4**, 1331.
14. W. Li, Q. Zhang, G. Zheng, Z. W. Seh, H. Yao and Y. Cui, *Nano Lett.*, 2013, **13**, 5534.
15. Y. S. Su and A. Manthiram, *Nat. Commun.*, 2012, **3**, 1166.
16. C. Huang, J. Xiao, Y. Shao, J. Zheng, W. D. Bennett, D. Lu, L. V. Saraf, M. Engelhard, L. Ji, J. Zhang, X. Li, G. L. Graff and J. Liu, *Nat. Commun.*, 2014, **5**, 3015.
17. Z. Lin, Z. Liu, W. Fu, N. J. Dudney and C. Liang, *Adv. Funct. Mater.*, 2013, **23**, 1064.
18. C.-P. Yang, S. Xin, Y.-X. Yin, H. Ye, J. Zhang and Y.-G. Guo, *Angew. Chem. Int. Ed.*, 2013, **52**, 8363.
19. A. Abouimrane, D. Dambournet, K. W. Chapman, P. J. Chupas, W. Weng and K. Amine, *J. Am. Chem. Soc.*, 2012, **134**, 4505.
20. L. Liu, Y. Hou, X. Wu, S. Xiao, Z. Chang, Y. Yang and Y. Wu, *Chem. Commun.*, 2013, **49**, 11515.
21. Y. Qu, Z. Zhang, S. Jiang, X. Wang, Y. Lai, Y. Liu and J. Li, *J. Mater. Chem. A*, 2014, **2**, 12255.
22. J. Zhang, Z. Zhang, Q. Li, Y. Qu and S. Jiang, *J. Electrochem. Soc.*, 2014, **161**, A2093.
23. C. Malitesta, I. Losito, L. Sabbatini and P. G. Zambonin, *J. Electron. Spectrosc. Relat. Phenom.*, 1995, **76**, 629.
24. Y. Li, Y. Zhao, H. Cheng, Y. Hu, G. Shi, L. Dai and L. Qu, *J. Am. Chem. Soc.*, 2012, **134**, 15.
25. L. F. Chen, X. D. Zhang, H. W. Liang, M. Kong, Q. F. Guan, P. Chen, Z. Y. Wu and S. H. Yu, *ACS Nano*, 2012, **6**, 7092.
26. D. Hulicova-Jurcakova, M. Seredych, G. Q. Lu and T. J. Bandosz, *Adv. Funct. Mater.*, 2009, **19**, 438.
27. L. Qie, W. M. Chen, Z. H. Wang, Q. G. Shao, X. Li, L. X. Yuan, X. L. Hu, W. X. Zhang and Y. H. Huang, *Adv. Mater.*, 2012, **24**, 2047.
28. R. Lukács, M. Veres, K. Shimakawa and S. Kugler, *J. Appl. Phys.*, 2010, **107**, 073517.
29. C. Luo, Y. Xu, Y. Zhu, Y. Liu, S. Zheng, Y. Liu, A. Langrock and C. Wang, *ACS Nano*, 2013, **7**, 8003.
30. J. L. K. F. Tuinstra, *J. Composite Mater.*, 1970, **4**, 492.
31. Y. Cui, A. Abouimrane, J. Lu, T. Bolin, Y. Ren, W. Weng, C. Sun, V. A. Maroni, S. M. Heald and K. Amine, *J. Am. Chem. Soc.*, 2013, **135**, 8047.
32. Z. Li, L.X. Yuan, Z.Q. Yi, Y.M. Sun, Y. Liu, Y. Jiang, Y. Shen, Y. Xin, Z. L. Zhang and Y.H. Huang, *Adv. Energ. Mater.*, 2014, **4**.
33. Y. P. Wu, C. Y. Jiang, C. R. Wang, S. B. Fang and Y. Y. Jiang, *J. Appl. Polym. Sci.*, 2000, **77**, 1735.